Nano Energy (▮▮▮▮) ▮, ▮▮▮–▮▮▮

Available online at www.sciencedirect.com

ScienceDirect

journal homepage: www.elsevier.com/locate/nanoenergy

RAPID COMMUNICATION

$Ni(OH)_2$@$Co(OH)_2$ hollow nanohexagons: Controllable synthesis, facet-selected competitive growth and capacitance property

Dan Zhou[a,b,1], Xinruo Su[a,1], Markus Boese[b], Rongming Wang[a,*], Hongzhou Zhang[b,*]

[a]Department of Physics, Beijing University of Aeronautics and Astronautics, Beijing 100191, PR China
[b]School of Physics & CRANN, Trinity College Dublin, Dublin 2, Republic of Ireland

Received 9 October 2013; received in revised form 13 January 2014; accepted 26 January 2014

KEYWORDS
Hollow hexagons;
Facet-selective growth;
Core–shell structure;
Capacitance property;
Longterm stability

Abstract

Hollow nanohexagons with a core-shell structure have been synthesized from a mixture of Ni and Co hydroxide by a mild wet chemical approach. $Ni(OH)_2$@$Co(OH)_2$ nanohexagons with controllable sizes of about 200 nm, morphology and structure are obtained. Comprehensive microstructure analysis reveals that the $Ni(OH)_2$ and $Co(OH)_2$ components are single-crystalline. The surfaces of the nanohexagons are smooth and their inner facets can be controlled to be parallel to the outer facets or rotated by 30°. A growth mechanism depending on the $N_2H_4 \cdot H_2O$ content and reaction temperature has been proposed to explain the different structures. The parallel inner facets tend to form with higher amounts of $N_2H_4 \cdot H_2O$ while the rotated ones tend to form at higher temperature. The specific capacitance of the hollow nanohexagon is about 369 F/g, which can be remained as high as 96.4% after 2500 cycles at current density of 1 A/g.

Introduction

A hollow nanohexagon is an universal fastener with six sides cut in a hexagonal shape, since it seems to be the easiest shape to grasp [1]. With its high torque resistance and small volume, these hexagons can be uniformly spaced on a planar surface and used in conjunction with a matching bolt to assemble mechanical mixtures. Many different nanostructures, such as nanoplates, nanotubes, nanorings, nanopillars and nanohelices [2–11], have been recognized, but the hollow nanohexagon is still a challenge. Great efforts have been made towards hollow nanohexagons. However, ideal hollow nanohexagons have never been reported. Similar nanostructures, such as such as nanosheets [12], nanoflake [9,13,14], and hollow nanostructures [15], [16–23] have widely been synthesized. It is

*Corresponding authors. Tel.: +86 10 8233 9567.
E-mail addresses: rmwang@buaa.edu.cn, rmwang@pku.edu.cn (R. Wang), hozhang@tcd.ie (H. Zhang).
[1]These authors contribute equally.

http://dx.doi.org/10.1016/j.nanoen.2014.01.006
2211-2855

Please cite this article as: D. Zhou, et al., $Ni(OH)_2$@$Co(OH)_2$ hollow nanohexagons: Controllable synthesis, facet-selected competitive growth and capacitance property, Nano Energy (2014), http://dx.doi.org/10.1016/j.nanoen.2014.01.006

necessary to produce uniform hexagonal structure with controllable size. Moreover, in the fields of electronics and semiconducting industries, it is also very important for the hollow hexagons to have unique electric and/or magnetic properties.

The challenge should be dealt with suitable materials and reaction conditions. Metal oxides or hydroxides with hexagonal crystal structure are potential candidates. Ferromagnetic transition elements, such as Fe, Co, and Ni, have been widely used for magnetic and spintronic applications. Their hydroxides, such as β-$Ni(OH)_2$, $Co(OH)_2$ crystalline with hexagonal brucite structure (space group $P\bar{3}ml$) have nearly identical lattice parameters and chemical properties [13,24-27], which makes them good candidates for hollow nanohexagons. Although composite Ni-Co hydroxides with diverse morphologies and self-assembled hierarchical structures, including flower-like nanosheets, [12] microspheres assembled from two-wheeled units, [24] porous nanoflake composite film, [13] and core-shell nanocolumns of $Ni(OH)_2$@$Co(OH)_2$, [14] etc. have been synthesized, hollow nanohexagons have never been reported. Here we describe a mild wet chemical synthesis of $Ni(OH)_2$@$Co(OH)_2$ hollow nanohexagons utilizing the difference in growth and/or dissolve speed for specific facets of $Ni(OH)_2$. The growth mechanism is proposed, and the electricity properties of the constructed nanohexagons have also been investigated.

Experimental methods

In a typical synthesis, $CoCl_2 \cdot 6H_2O$ and $NiCl_2 \cdot 6H_2O$ with a molar ratio of 9:1 were dissolved in de-ionized water. $N_2H_4 \cdot H_2O$ (80 wt%, 0.1-0.5 ml) was added to the solution as reducing agent. During the reaction, the pH value of the solution was kept at 13 by adding NaOH. The solution was stirred for 5 min at room temperature and then heated at 120-180 °C for 6 h in a sealed Teflon-lined autoclave. The autoclave was then cooled to room temperature in air. The product was collected by centrifugation and washed several times with de-ionized water and ethanol with further centrifugation.

The overall crystallinity and phase purity of the as-synthesized samples were analyzed by X-ray powder diffraction on a Rigaku Dmax 2200 X-ray diffractometer using Cu K_α incident radiation. The morphologies and chemical compositions of the products were characterized by a Hitachi S-4800 scanning electron microscope (SEM) and a Carl Zeiss Ultra SEM equipped with an Oxford X-max energy-dispersive spectrometer (EDS). The crystal structure and elemental distribution are analyzed on an FEI Titan transmission electron microscope (TEM, 300 kV) equipped with a Gatan electron energy filter to record electron energy-loss spectra (EELS) and energy-filtered TEM micrographs (EFTEM). Cyclic voltammetry (CV) tests and chronopotentiometry (CP) tests were performed on CHI660D electrochemical workstation. The electrochemical measurements were carried out in a three-electrode electrochemical cell containing 6 M KOH aqueous solution as electrolyte. The specific surface areas of the hollow nanohexagons were determined by the Brunauer-Emmett-Teller (BET) measurement.

Results and discussion

The as-synthesized material was first identified as Ni-Co hydroxide by X-ray diffraction (XRD) and energy dispersive X-ray spectroscopy (EDS). As shown in Figure 1(a), the X-ray diffraction pattern of the typical products exhibited a typical pattern similar to that of $Co(OH)_2$ and β-$Ni(OH)_2$. Small-size effects were shown by the broadened peak widths. By using the Scherer formula, $d=0.89\lambda/(\beta \cos\theta_B)$, where λ is the X-ray wavelength (0.15406 nm), θ_B is the Bragg diffraction angle, and β is the peak width at half-maximum, the (101) peak in Figure 1(a) gives a characteristic size of about 25 ± 8 nm.

Figure 1(b-e) demonstrate that the Ni-Co hydroxides synthesized hollow nanohexagons were very uniform. It is interesting to point out that two kinds of hollow nanohexagons can be obtained under different conditions. As shown in Figure 1(b) and (c), the inner facets of the hollow nanohexagons synthesized with 0.4 ml $N_2H_4 \cdot H_2O$ at 120 °C

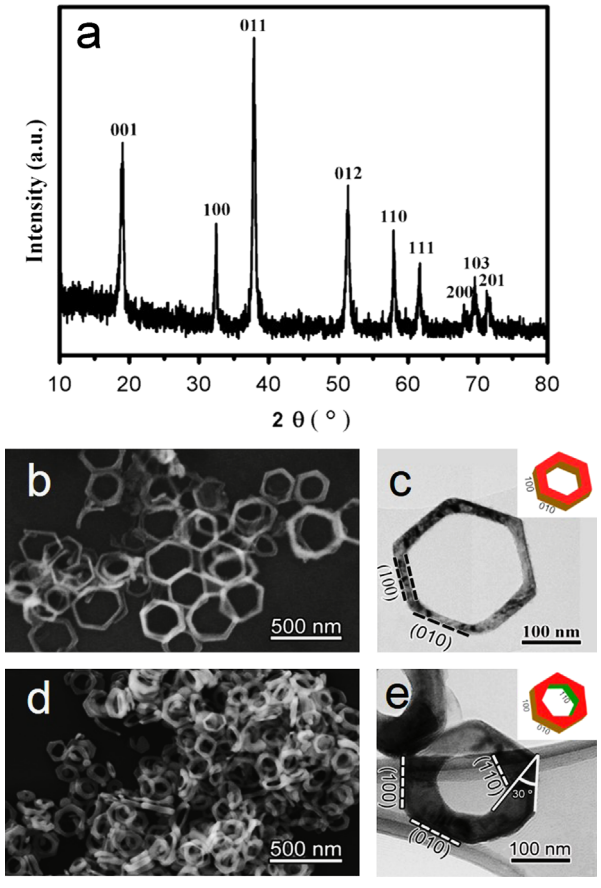

Figure 1 (a) XRD spectra of samples synthesized at 120 °C with 0.1 ml reducing agent; (b) SEM image of a $Co(OH)_2/Ni(OH)_2$ hollow nanohexagons synthesized at 120 °C with 0.4 ml reducing agent; (c) TEM bright-field image of a $Co(OH)_2/Ni(OH)_2$ hollow nanohexagons synthesized at 120 °C with 0.4 ml reducing agent; (d) SEM image of $Co(OH)_2/Ni(OH)_2$ hollow nanohexagons synthesized at 180 °C with 0.1 ml reducing agent; (d) TEM bright-field image of $Co(OH)_2/Ni(OH)_2$ hollow nanohexagons synthesized at 180 °C with 0.1 ml reducing agent; The inserts show the crystal structure model of the hollow nanohexagon of the corresponding TEM images.

Please cite this article as: D. Zhou, et al., $Ni(OH)_2$@$Co(OH)_2$ hollow nanohexagons: Controllable synthesis, facet-selected competitive growth and capacitance property, Nano Energy (2014), http://dx.doi.org/10.1016/j.nanoen.2014.01.006

are found to be parallel with the outer facets. Scanning electron microscopy (SEM, Figure 1(b)) and transmission electron microscopy (TEM, Figure 1(c)) images indicate that the products have a typical hexagonal structure with uniform size ~200 nm and morphology. The diameters of the nanohexagons depend on the quantity of reducing agent and reaction temperature. The diameters of the nanohexagons change from 193 ± 19 nm with 0.1 ml $N_2H_4\cdot H_2O$ to (263 ± 10) nm with 0.5 ml $N_2H_4\cdot H_2O$. For the products synthesized with 0.4 ml $N_2H_4\cdot H_2O$ at 120 °C, the walls exhibit ideal hexagonal structure with wall thickness measured to be 26 ± 6 nm, which matches with the characteristic size calculated from XRD results.

Investigations indicate that the morphology of the nanohexagons can also be controlled by adjusting the amount of $N_2H_4\cdot H_2O$ during the reaction. Figure S1 shows the SEM images of the products synthesized with reducing agent varied from 0.1 ml to 0.5 ml at 120 °C. With the increase of the reducing agent, the products change from pure hexagonal nanodiscs (0.1 ml) via a mixture of nanodiscs and nanohexagons (0.2–0.3 ml) and to pure nanohexagons ($\geq$0.4 ml). Further increase of the reducing agent amount will break the nanohexagons. The morphology evolution of the nanostructures via the amount of the reducing agent is also studied by measuring the wall thickness of the nanohexagons averaging from over 100 randomly picked nanostructures. As shown in Figure S1(f), the wall thickness of the nanohexagons decreases from 42 ± 5 nm to 24 ± 3 nm with the increase of the reducing agent from 0.3 ml to 0.5 ml. EDS analysis reveals that Co:Ni ratio in the product decreases linearly from 9:1 to about 1:2 with increasing reducing agent amount.

Bright-field TEM image (Figure 1(c)) and corresponding diffraction pattern of the nanohexagons reveal the single crystal nature of the nanohexagons. The TEM image and the diffraction pattern were taken along the [001] zone axis. By correlating the bright-field TEM image and the diffraction pattern, it can be concluded that the sidewalls of the Ni-Co hydroxides hollow nanohexagons are terminated by {100} planes. The crystallographic structure of the nanohexagon is illustrated in the inset of Figure 1(c).

We find that the reaction temperature can also modify the crystallographic structure. Figure 1(d) and (e) shows SEM and TEM images of the nanohexagons synthesized with 0.1 ml $N_2H_4\cdot H_2O$ at 180 °C. It is interesting to see that the inner hexagonal facets are not parallel with the outer ones as in the products synthesized at 120 °C. Instead, the two hexagons were placed with the vertexes pointing to the middle of the edges, keeping six-fold symmetry of the nanostructure. In other words, the two facets of the two hexagons are rotated by 30° with each other. In order to keep the structure, the wall thickness became wider compared with the parallel ones. However, if we measure the distance from the vertex of the inner hexagon to the edge of the outer one, the distance can also be controlled similarly to the characteristic size of the nanohexagons, as indicated by XRD.

Figure S2 shows the SEM images of the products synthesized with reaction temperature varied from 120 °C to 180 °C. With the increase of temperature, the products change from pure hexagonal nanodiscs (120 °C) via the mixture of nanodiscs and nanohexagons (150 °C) and to pure nanohexagons (180 °C). Further increase of the temperature will lead to different nanostructures. The evolution of the morphology via the reaction temperature was also studied by measuring the distance from the inner vertexes to the outer edge of the nanohexagons averaged over 100 randomly picked nanostructures. As shown in Figure S2(d), the distance decreases from 35 ± 4 nm to 27 ± 3 nm as the temperature is increased from 150 °C to 180 °C.

At elevated reaction temperature, the production rate of the nanohexagons decreased. EDS analysis reveals that Co:Ni ratio in the product decreases linearly from 9:1 to about 1:5 with 0.1 ml $N_2H_4\cdot H_2O$ as the reaction temperature is increased from 120 °C to 180 °C. Excess addition of $N_2H_4\cdot H_2O$ will even decrease the yield.

TEM image (Figure 1(e)) and the corresponding diffraction pattern of the nanohexagon synthesized at 180 °C also confirms the single-crystalline nature of the products. Following the analysis in Figure 1(c), the surface of the Ni-Co hydroxide nanohexagons are terminated by hexagonal {100} planes as before. The inner facets of the nanohexagons are found to be terminated by {110} planes. The crystallographic structure of the nanohexagon is illustrated in the inset of Figure 1(e).

As indicated in the XRD patterns, the hollow nanohexagons consist of $Ni(OH)_2$ and $Co(OH)_2$ with the same space group ($P\bar{3}ml$) and almost identical lattice parameter (Lattice Difference $\leq$ 0.006 nm). [28,29] Normal high resolution TEM and selected area diffraction (Figure S3) have difficulty to distinguish them. Then EFTEM analysis was conducted to reveal the elemental distribution within a nanohexagon, following our previous work on BCN nanotube. [30] Both kinds of nanohexagons are investigated, as shown in Figure 2. Figure 2(a) shows a bright-field TEM image with elemental mapping of the nanohexagons synthesized with 0.4 ml N_2H_4•H_2O at 120 °C. The elemental mappings of nickel, cobalt and oxygen are rendered with different colors. The green color in the shell of the nanohexagon represents cobalt, the red color in the inner layer represents nickel and the blue color throughout the entire nanohexagon represents oxygen. The results indicate that the Ni-Co hydroxides form a core-shell structure with a $Ni(OH)_2$ core and a $Co(OH)_2$ shell.

The relatively larger lattice parameter of $Co(OH)_2$ (a=0.3186 nm, c=0.4653 nm) compared with that of $Ni(OH)_2$ (a=0.3127 nm, c=0.4606 nm) may be responsible for the formation of core-shell structure, similar to FePt nanoparticles with a compressed core and expanded shell [15,31]. Despite of the different inner facets, the elemental mapping of the nanohexagon synthesized with 0.4 ml N_2H_4•H_2O at 120 °C is $Ni(OH)_2$@$Co(OH)_2$ reveals a similar structure. As demonstrated in Figure 2(b), the nanohexagons all have $Ni(OH)_2$ cores and $Co(OH)_2$ shells, so the structure can be described as $Ni(OH)_2$@$Co(OH)_2$. The only difference is that the wall of the nanohexagon with inner hexagon rotated 30° with respect to the outer one becomes thicker to meet the rotation requirement between them. However, the smallest distance in the rotated nanohexagon can be as small as that of the parallel one.

Based on the above characterization, a possible growth mechanism for the evolution from $Co_{0.9}Ni_{0.1}(OH)_2$ nanoplates to facet-selective formation of core-shell $Ni(OH)_2$@$Co(OH)_2$

Please cite this article as: D. Zhou, et al., $Ni(OH)_2$@$Co(OH)_2$ hollow nanohexagons: Controllable synthesis, facet-selected competitive growth and capacitance property, Nano Energy (2014), http://dx.doi.org/10.1016/j.nanoen.2014.01.006

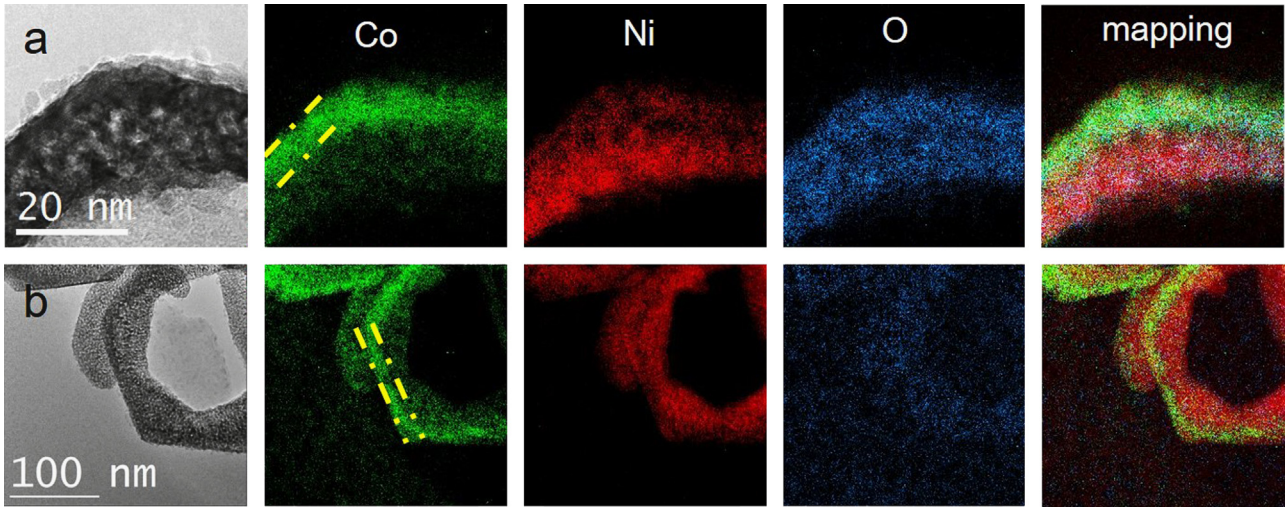

Figure 2 (a) TEM bright-field image of a nanohexagon synthesized at 120 °C with 0.4 ml reducing agent and its corresponding EFTEM mapping of Co, Ni, O and general view; (b) TEM bright-field image of a nanohexagon synthesized at 180 °C with 0.1 ml reducing agent and its corresponding EFTEM mapping of Co, Ni, O and general view.

hollow nanohexagons with the variation of the amount of reducing agent or reaction temperature may be proposed. Both internal crystal factors and external factors, such as the additives [32], reaction time [5,33] and reaction temperature [34–36] should be considered.

The formation of core-shell $Ni(OH)_2@Co(OH)_2$ nanohexagons can be divided into three steps: (I) formation of $Co(OH)_2/Ni(OH)_2$ nuclei, (II) formation of $Co_{0.9}Ni_{0.1}(OH)_2$ nanoplates and (III) formation of $Ni(OH)_2@Co(OH)_2$ nanohexagons. The reaction process in steps II and III can be described as the following equations:

$$0.9CoCl_2 \cdot 6H_2O + 0.1NiCl_2 \cdot 6H_2O + 2NaOH = Co_{0.9}Ni_{0.1}(OH)_2 + 12H_2O + 2NaCl \quad (1)$$

$$Co_{0.9}Ni_{0.1}(OH)_2 + 0.5xN_2H_4 \cdot H_2O = xCo + 0.1Ni(OH)_2@(0.9\text{-}x)Co(OH)_2 + 0.5xN_2\uparrow + 2.5xH_2O \ (0 \le x \le 0.9) \quad (2)$$

x is the fraction of Co ions in the precursors.

In formation step II, the Co-Ni hydroxide nanoplate tends to grow along the [001] zone axis to form hexagonal structure. In step III, facet-selective reaction begins from the center of the hexagonal nanoplate to form the hollow nanohexagon. The formation of the nanohexagons is schematically illustrated in Figure 3.

In the current synthesis system, $N_2H_4 \bullet H_2O$ acts as a strong reducing agent. Co/Ni hydroxide tends to be reacted first, as expressed by Eq. (1). [37] Since Co/Ni hydroxide has a hexagonal brucite structure (Figure 3(a)), it can form thermodynamically stable hexagonal thin sheets built an n intrinsic lamellar structure, as shown in Figure 3(b). Unlike the reported synthesis of $Ni(OH)_2$ and $Co(OH)_2$ nanoplates, [14] in which Co ions were added after the formation of Ni $(OH)_2$, mixed Ni ions and Co ions were added before the introduction of any other reactant in our case. SEM and TEM investigations indicate that the reaction occurs when the temperature exceeds 120 °C. In this step, hexagonal $Co_{0.9}Ni_{0.1}(OH)_2$ nanoplates with a homogeneous distribution of Ni and Co were formed.

Previous reports indicated that a higher density of imperfections, such as surface roughness, [35] planar defects, [36] and a high surface tension, [38] exist near the center of the nanoplates. The imperfections reduce the dissolution energy of the nanocrystals, and thus a higher dissolution rate is possible in the center of the nanoplates (Figure 3(c)). With the addition of reducing agent, the nanoplate begins to dissolve from the center according to Eq. (2). Then nanoscale holes will form near the center of the nanoplates, as shown in Figure 3(d). The nanoscale holes will connect to form a big hole. With prolonged reaction time, the hole becomes gradually larger and finally results in the formation of the nanohexagon. The observed hexagonal holes in the products reveals that the facet-selected growth dominates.

As expressed in Eq. (2), Co^{2+} is more easily to grow from the hydroxide than Ni^{2+}. During the reaction, the $Co_{0.9}Ni_{0.1}(OH)_2$ precursor was reduced to metallic Co and a $Ni(OH)_2$ core formed in the center. With the reaction proceed, the content of Ni^{2+} in the precursor decreased. In the end the Ni^{2+} in the precursor was exhausted and Co $(OH)_2$ shell was formed. Such element distribution has been confirmed by EFTEM analysis.

Previous reports [28] indicated that the bonds between certain ions and {110} facets of a hexagonal Fe_2O_3 would be strengthened at increased temperature. In our case, when the reaction temperature was increased from 120 °C to 180 °C, the bond between the ions and {110} facets of Ni $(OH)_2$ is more strengthened than that between the ions and {100} facets at the stabilization period, which result in the formation of hexagon terminated with six equivalent {100} facets. It should also be noted that in this case, the stress resulting from the lattice difference of $Ni(OH)_2$ and $Co(OH)_2$ may be minimized in the $Ni(OH)_2@Co(OH)_2$ hollow nanohexagons. As shown in Figure S3, the stress observed from the contrast in the HRTEM image of the nanohexagons is relaxed.

The electrochemistry of the $Ni(OH)_2@Co(OH)_2$ nanohexagons has also been investigated. As shown in Figure 4, cyclic voltammetry (CV) and chronopotentiometry (CP) experiments were performed. The working electrode was prepared by mixing $Ni(OH)_2@Co(OH)_2$ hollow nanohexagons

Please cite this article as: D. Zhou, et al., $Ni(OH)_2@Co(OH)_2$ hollow nanohexagons: Controllable synthesis, facet-selected competitive growth and capacitance property, Nano Energy (2014), http://dx.doi.org/10.1016/j.nanoen.2014.01.006

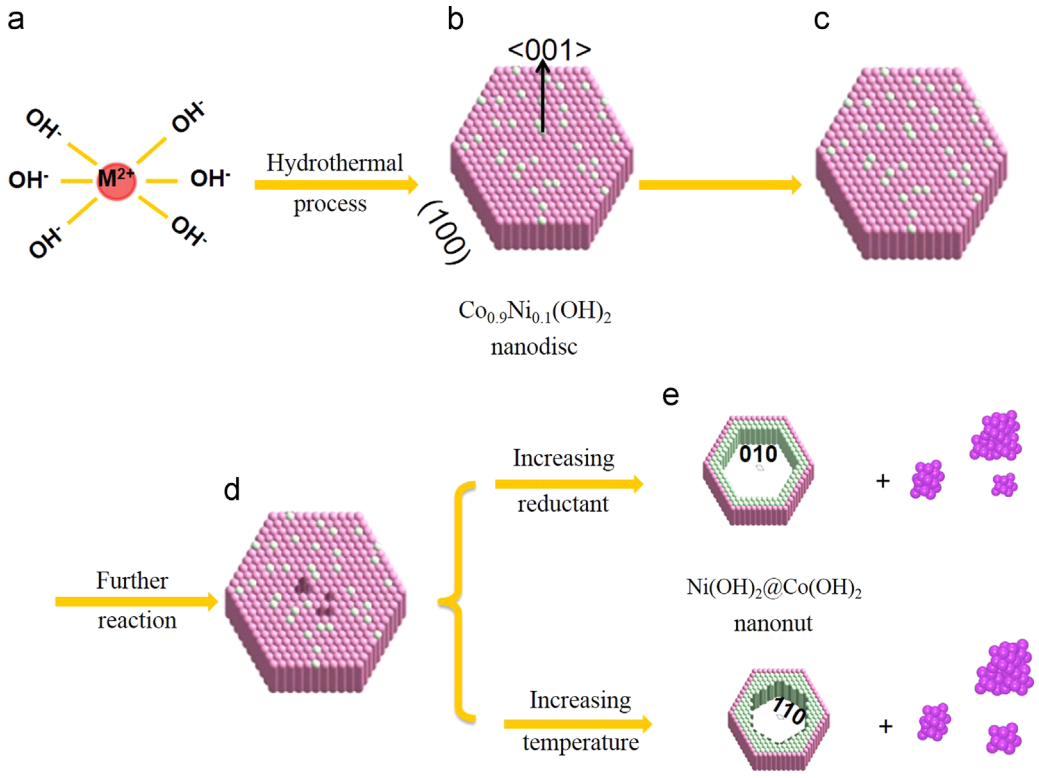

Figure 3 Schematic view of the formation process of the nanoplates and the nanohexagons. In (b), (c), (d) and (e), pink color represents Co's distribution and green color represents Ni's distribution.

(synthesized with 0.4 ml $N_2H_4 \cdot H_2O$ at 120 °C), carbon black and polytetrafluoroethylene in a weight ratio of 7:2:1 and pressing the mixture into a nickel foam. As shown in Figure 4(a), the cyclic voltammogram consist of two pairs of redox couples. The CV curves have changed in different scanning rates. The reduction peaks P1 (−0.02 V) and P2 (+0.229 V) and oxidation peaks P3 (+0.053 V) and P4 (+0.319 V) vs Ag/AgCl can be distinguished out. The shape of the CV curve in Figure 4(a) is quite different to that of a double layer capacitor, which indicates that the capacitance characteristics of these two pairs of redox couples are governed by Faradaic reactions [39]. In anodic process, Co^{2+} shift to Co^{3+} and Co^{4+} step by step, and in cathodic process, the Co^{4+} shifts to Co^{2+}. The redox peaks, P1 and P3, can be attributed to the valence state changes between Co^{2+} and Co^{3+}, which can be described by the following equation:

$$Co(OH)_2 + OH^- \leftrightarrow CoOOH + H_2O + e^- \quad (6)$$

Another couple of redox peaks, P2 and P4 in Figure 4 can be attributed to the changes between Co^{3+} and Co^{4+}, which can be described as:

$$CoOOH + OH^- \leftrightarrow CoO_2 + H_2O + e^- \quad (7)$$

In our nanostructure, the $Ni(OH)_2$ shell should also be considered in the redox reaction, [38], [39] which can be described as

$$Ni(OH)_2 + OH^- \leftrightarrow NiOOH + H_2O + e^- \quad (8)$$

The redox potentials between Ni^{2+} and Ni^{3+} are close to those between Co^{3+} and Co^{4+} (P2 and P4). Their coupling makes the P2 and P4 peaks in Figure 4(a) pronounced.

Specific capacitance can be calculated from the CV curves in Figure 4(a) using the following formula:

$$C_v = \frac{\int I\,dt}{m\Delta V} \quad (9)$$

where I is the current density, dt is the time differential, m is the mass of electroactive material and ΔV is the range of potential window. The average specific capacitance of the nanohexagons is calculated to be ~302 F/g at a scanning rate of 5 mV/s. At higher scanning rate, the average specific capacitance is found to decrease exponentially (Figure 4(c)), indicating incomplete charging at higher scanning rate. [40]

Figure 4(b) demonstrates the chronopotentiometric behavior of the nanohexagons electrode between −0.1 V and +0.40 V at various current densities, as indicated, in 6 M KOH electrolyte. The shape of the CP curves mainly shows its capacitive characteristic, which corresponds with the CV curves.

The specific capacitance of the nanohexagons can also be obtained by chronopotentiometric experiment. It can be calculated by the following equation:

$$C_p = \frac{I\Delta t}{m\Delta V} \quad (10)$$

where I is the constant charge/discharge current, m is the mass of electroactive material, Δt is the total discharge time and ΔV is the range of the potential window during discharge. Figure 4(b) depicts the chronopotentiometric spectra of the synthesized nanohexagons at current densities of 0.3 A/g, 0.5 A/g and 1 A/g. The corresponding specific capacitances are calculated to be 369 F/g,

Please cite this article as: D. Zhou, et al., $Ni(OH)_2$@$Co(OH)_2$ hollow nanohexagons: Controllable synthesis, facet-selected competitive growth and capacitance property, Nano Energy (2014), http://dx.doi.org/10.1016/j.nanoen.2014.01.006

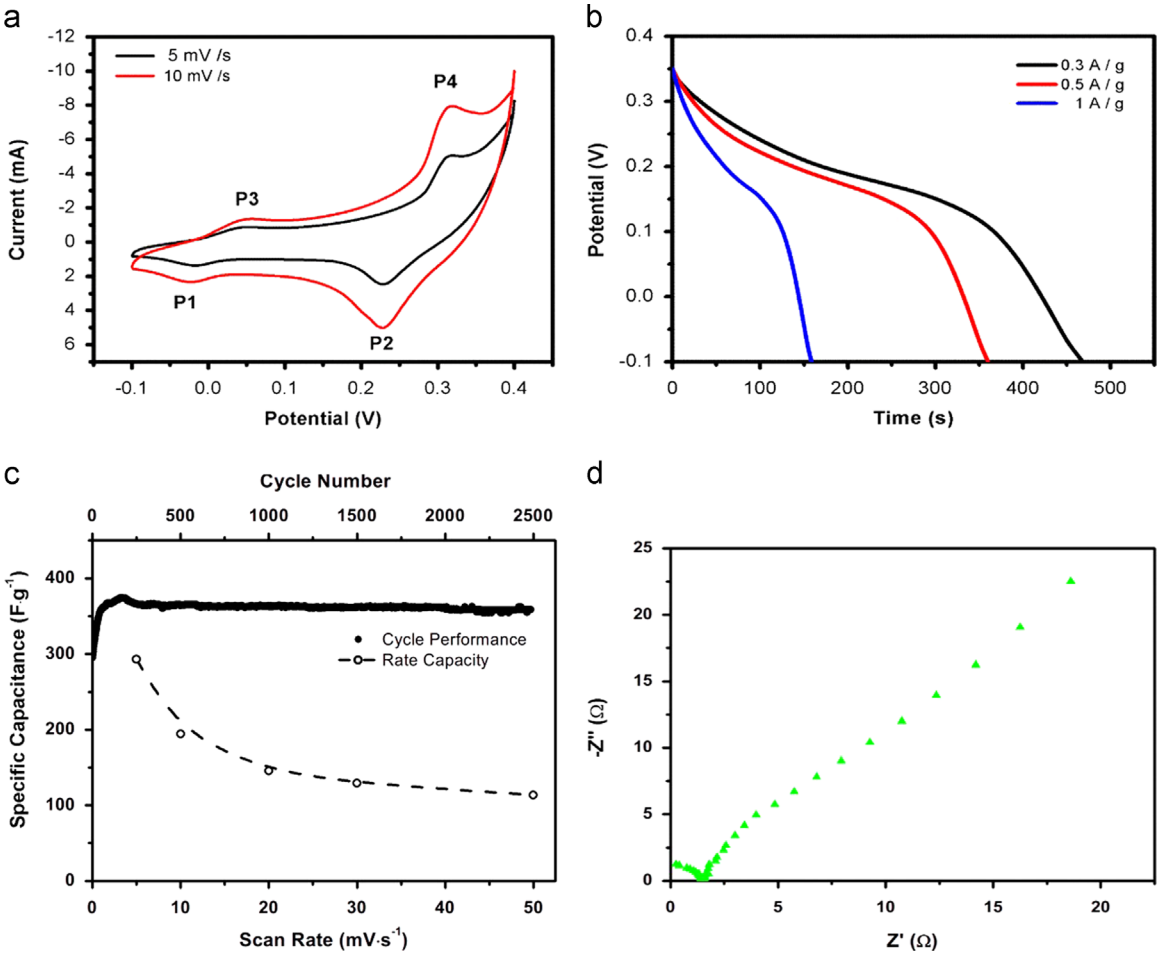

Figure 4 (a) Cyclic voltammogram of the core-shell $Ni(OH)_2$@$Co(OH)_2$ hollow nanohexagons at scanning rate of 5 mV/s and 10 mV/s. (b) Discharge curves of the core-shell $Ni(OH)_2$@$Co(OH)_2$ hollow nanohexagons at different current densities. (c) Specific capacitance of core-shell $Ni(OH)_2$@$Co(OH)_2$ hollow nanohexagons as functions of cycle number and scan rate tested in 6M KOH electrolyte. (d) Impedance spectra of the core-shell $Ni(OH)_2$@$Co(OH)_2$ hollow nanohexagons electrodes.

367 F/g and 312 F/g, respectively. The value of the specific capacitance at higher current density (1 A/g) is found to be significantly smaller than those at lower current densities (0.3 A/g and 0.5 A/g), indicating incomplete charging during the process. If you compare the specific capacitance (312 F/g) at current density of 1 A/g using chronopotentiometric measurement with that (302 F/g) obtained from CV measurement at scanning rate of 5 mV/s, you can found that they have similar values, indicating similar charging performance in these two experiments. Moreover, the similarity of the values at lower current densities (0.3 A/g and 0.5 A/g) indicate almost complete charging performance during these processes. Then the value measured at current density of 0.3 A/g using chronopotentiometric measurement can represent the specific capacitance of the synthesized hollow nanohexagons.

As the specific capacitance of the material is greatly influenced by its specific area [41,42], a BET (Brunauere-Emmett-Teller) measurement was taken to measure the specific surface area of the synthesized nanohexagons. The obtained specific surface area of 23.3 m^2/g is found to be only little higher than the theoretical one ~21.2 m^2/g calculated from the observed geometry by SEM and TEM, revealing excellent smooth surfaces of the synthesized nanohexagons. Then the area specific capacitance of the $Ni(OH)_2$@$Co(OH)_2$ nanohexagons can be calculated to be ~15.8 F/m^2, which is comparable to the value of $Ni(OH)_2$ (16.9 F/m^2) [43] and about three times of the value of $Co(OH)_2$ (~5.4 F/m^2) [42]. The result indicates the synthesized $Ni(OH)_2$@$Co(OH)_2$ nanohexagons can keep high specific capacitance, which may be attributed to the synergy effect in the core@shell structure.

The cycling performance of supercapacitor using hollow nanohexagon was examined in 6M KOH electrolyte at current density of 1 A g^{-1} and the result is depicted in Figure 4(c). It can be found that the nanohexagons exhibit extraordinary stability in KOH electrolyte solution. After 2500 cycles, the specific capacitance (~358 F/g) still remains over 95% of the maximum capacitance.

The electrochemical impedance spectroscopy (EIS) analysis measurement was taken and corresponding Nyquist plot is shown in Figure 4(d). In the high frequency area, the intersection of the curve at real part Z′ indicates the bulk resistance of the electrochemical system, and the semicircle displays the charge-transfer process along the working electrode-electrolyte interface. The result indicates that the hollow nanohexagon has excellent charge transfer

Please cite this article as: D. Zhou, et al., $Ni(OH)_2$@$Co(OH)_2$ hollow nanohexagons: Controllable synthesis, facet-selected competitive growth and capacitance property, Nano Energy (2014), http://dx.doi.org/10.1016/j.nanoen.2014.01.006

property compared with other $Co(OH)_2$ or $Ni(OH)_2$ nanostructures. The charge transfer resistance (1.48 Ω) of the synthesized $Ni(OH)_2$@$Co(OH)_2$ nanohexagons is only about 12% of the Ni-doped $Co(OH)_2$/ITO nanowires (12.8 Ω). [44] In low frequency area, the slope of the curve shows the Warburg impedance which represents the electrolyte diffusion in the electrode and proton diffusion in the nanohexagons. The slope of the straight line in the low frequency region is larger than that of the 45° straight line, indicating typical capacitor behavior [45].

Conclusions

Facet-selective growth of core–shell $Ni(OH)_2$@$Co(OH)_2$ hollow nanohexagons has been achieved by controlling the temperature and the amount of $N_2H_4 \cdot H_2O$ in a facile hydrothermal synthesis. The SEM results indicate that the increase of both of these parameters can change the product morphology from hexagonal nanoplates to hollow nanohexagons. XRD, EDS, and EFTEM analyses showed that the formation of nanohexagons is accompanied by the precipitate of metallic Co from the nanoparticles in a shell-shrinking way, which directly leads to separation of the Co and Ni in the particle. Further TEM characterization revealed that, the inner facets of the nanohexagons were {100} planes when the amount of reducing agent was increased from 0.1 mL to 0.5 mL at 120 °C, and {110} planes when the reaction temperature was increased from 120 °C to 180 °C with 0.1 ml N_2H_4•H_2O. It is interesting that the inner facets of the hollow nanohexagons can be controlled to be parallel to the outer facets or rotated by 30° by controlling the amounts of $N_2H_4 \cdot H_2O$. The synthesized $Ni(OH)_2$@$Co(OH)_2$ nanohexagons can keep high specific capacitance of ~369 F/g, which is similar to $Ni(OH)_2$ and about three times of $Co(OH)_2$. It exhibits extraordinary long-term electrochemical stability with specific capacitance maintained over 95% of the maximum capacitance after 2500 cycles in alkaline solution. It also exhibits excellent charge transfer property with resistant of only 1.48 Ω.

Uncited references

[25], [26], [27], [37].

Acknowledgment

The authors thank Professor J.M.D. Coey from Trinity College Dublin, Ireland for useful discussion and instruction for the paper. This work is supported by the National Natural Science Foundation of China (NSFC 51371015, 11174023, 51331002), the Beijing Municipal research project for outstanding doctoral thesis supervisors (20121000603), and Science Foundation Ireland under Grant 07/SK/I1220a. The TEM work was conducted under the framework of the INSPIRE program, funded by the Irish Government's Program for Research in Third Level Institutions, Cycle 4, National Development Plan 2007–2013.

Appendix. Supporting information

Supplementary data associated with this article can be found in the online version at http://dx.doi.org/10.1016/j.nanoen.2014.01.006.

References

[1] ⟨http://www.wisegeek.com/what-is-a-hexagonal-nut.htm⟩.
[2] Y. Cui, Q.Q. Wei, H.K. Park, C.M. Lieber, Science 293 (2001) 1289–1292.
[3] X.W. Xie, Y. Li, Z.Q. Liu, M. Haruta, W.J. Shen, Nature 458 (2009) 746–749.
[4] R.H. Baughman, A.A. Zakhidov, W.A. de Heer, Science 297 (2002) 787–792.
[5] S. Jung, W. Cho, H.J. Lee, M. Oh, Angew Chem.-Int. Ed. 48 (2009) 1459–1462.
[6] X.Y. Kong, Y. Ding, R. Yang, Z.L. Wang, Science 303 (2004) 1348–1351.
[7] P.X. Gao, Y. Ding, W. Mai, W.L. Hughes, C. Lao, Z.L. Wang, Science 309 (2005) 1700–1704.
[8] Y. Song, S. Ji, Y.-J. Song, R. Li, J. Ding, X. Shen, R. Wang, R. Xu, X. Gu, J. Phys. Chem. C 117 (2013) 17274–17284.
[9] R.M. Wang, Y.J. Xing, J. Xu, D.P. Yu, N. J. Phys. 5 (2003) 115.
[10] R. Kapadia, Z. Fan, K. Takei, A. Javey, Nano Energy 1 (2012) 132–144.
[11] B. Hua, B. Wang, M. Yu, P.W. Leu, Z. Fan, Nano Energy 2 (2013) 951–957.
[12] X.L. Huang, X. Zhao, Z.L. Wang, L.M. Wang, X.B. Zhang, J.f Mater. Chem. 22 (2012) 3764–3769.
[13] X.H. Xia, J.P. Tu, Y.Q. Zhang, Y.J. Mai, X.L. Wang, C.D. Gu, X.B. Zhao, J. Phys. Chem. C 115 (2011) 22662–22668.
[14] M. Yao, W.M. Chen, X. Fan, C.M. Liu, X.M. Meng, L. Guo, C.P. Chen, CrystEngComm 13 (2011) 2593–2598.
[15] R.M. Wang, O. Dmitrieva, M. Farle, G. Dumpich, H.Q. Ye, H. Poppa, R. Kilaas, C. Kisielowski, Phys. Rev. Lett. 100 (2008) 017205.
[16] Y.Q. Shen, J.Z. Yin, F. Gao, J.J. Wang, H.A. Pang, Q.Y. Lu, Chem. Commun. 46 (2010) 6183–6185.
[17] S. Sitaula, M.R. Mackiewicz, S.M. Reed, Chem. Commun. (2008) 3013–3015.
[18] B.T. Qiao, A.Q. Wang, X.F. Yang, L.F. Allard, Z. Jiang, Y.T. Cui, J.Y. Liu, J. Li, T. Zhang, Nat. Chem. 3 (2011) 634–641.
[19] C. Peng, L. Gao, S. Yang, Chem. Commun. (2007) 4372–4374.
[20] Y.D. Yin, R.M. Rioux, C.K. Erdonmez, S. Hughes, G.A. Somorjai, A.P. Alivisatos, Science 304 (2004) 711–714.
[21] B. Tao, Q. Zhang, Z.Z. Liu, B.Y. Geng, Mater. Chem. Phys. 136 (2012) 604–612.
[22] Q. Sun, Z. Ren, R. Wang, N. Wang, X. Cao, J. Mater. Chem. 21 (2011) 1925–1930.
[23] R. Jing, A.X. Shan, R.M. Wang, C.P. Chen, CrystEngComm 15 (2013) 3587–3592.
[24] H.Y. Gao, G. Wang, M. Yang, L. Tan, J. Yu, Nanotechnology 23 (2012) 015607.
[25] W.H. Chen, Y.F. Yang, H.X. Shao, J. Fan, J. Phys. Chem. C 112 (2008) 17471–17477.
[26] J.X. Li, M. Yang, J.P. Wei, Z. Zhou, Nanoscale 4 (2012) 4498–4503.
[27] L.H. Su, L.Y. Gong, J.L. Gao, J. Power Sources 209 (2012) 141–146.
[28] B.L. Lv, Y. Xu, D. Wu, Y.H. Sun, Chem. Commun. 47 (2011) 967–969.
[29] F. Pertlik, Monatshefte Chem. 130 (1999) 1083–1088.
[30] R.M. Wang, H.Z. Zhang, N. J. Phys. 6 (2004) 78.

[31] R.M. Wang, O. Dmitrieva, M. Farle, G. Dumpich, M. Acet, S. Mejia-Rosales, E. Perez-Tijerina, M.J. Yacaman, C. Kisielowski, J. Phys. Chem. C 113 (2009) 4395–4400.
[32] Y. Peng, A.W. Xu, B. Deng, M. Antonietti, H. Colfen, J. Phys. Chem. B 110 (2006) 2988–2993.
[33] Q. Dong, N. Kumada, Y. Yonesaki, T. Takei, N. Kinomura, Mater. Res. Bull. 46 (2011) 1156–1162.
[34] Q. Peng, Y.J. Dong, Y.D. Li, Angew. Chem.-Int. Ed. 42 (2003) 3027–3030.
[35] F. Li, Y. Ding, P.X.X. Gao, X.Q. Xin, Z.L. Wang, Angew. Chem.-Int. Ed. 43 (2004) 5238–5242.
[36] W.Z. Wang, D. Long, Y.J. Liang, G.L. Zhang, B.Q. Zeng, Q.Y. He, Langmuir 27 (2011) 815–819.
[37] H.I. Won, H.H. Nersisyan, C.W. Won, Mater. Chem. Phys. 133 (2012) 225–231.
[38] H. Yoo, J. Sharma, J.K. Kim, A.P. Shreve, J.S. Martinez, Adv. Mater. 23 (2011) 44314434.
[39] F. Tao, Y. Shen, Y. Liang, H. Li, J. Solid State Electron. 11 (2006) 853–858.
[40] X. Xia, J. Tu, Y. Zhang, X. Wang, C. Gu, X.-b. Zhao, H.J. Fan, ACS Nano 6 (2012) 5531–5538.
[41] C.-Y. Sun, Y.-G. Zhu, T.-J. Zhu, J. Xie, G.-S. Cao, X.-B. Zhao, J. Solid State Electrochem. 17 (2013) 1159–1165.
[42] F. Cao, G.X. Pan, P.S. Tang, H.F. Chen, J. Power Sources 216 (2012) 395–399.
[43] X. Sun, G. Wang, H. Sun, F. Lu, M. Yu, J. Lian, J. Power Sources 238 (2013) 150–156.
[44] D. Tai Dam, J.-M. Lee, Nano Energy 2 (2013) 1186–1196.
[45] Q. Wang, X. Wang, B. Liu, G. Yu, X. Hou, D. Chen, G. Shen, J. Mater. Chem. A 1 (2013) 2468–2473.

Please cite this article as: D. Zhou, et al., $Ni(OH)_2@Co(OH)_2$ hollow nanohexagons: Controllable synthesis, facet-selected competitive growth and capacitance property, Nano Energy (2014), http://dx.doi.org/10.1016/j.nanoen.2014.01.006